Biophysical Journal, Volume 99

Supporting Material

On the Roles of Substrate Binding and Hinge Unfolding in Conformational Changes of Adenylate Kinase

Jason B. Brokaw and Jhih-Wei Chu

CONTENTS

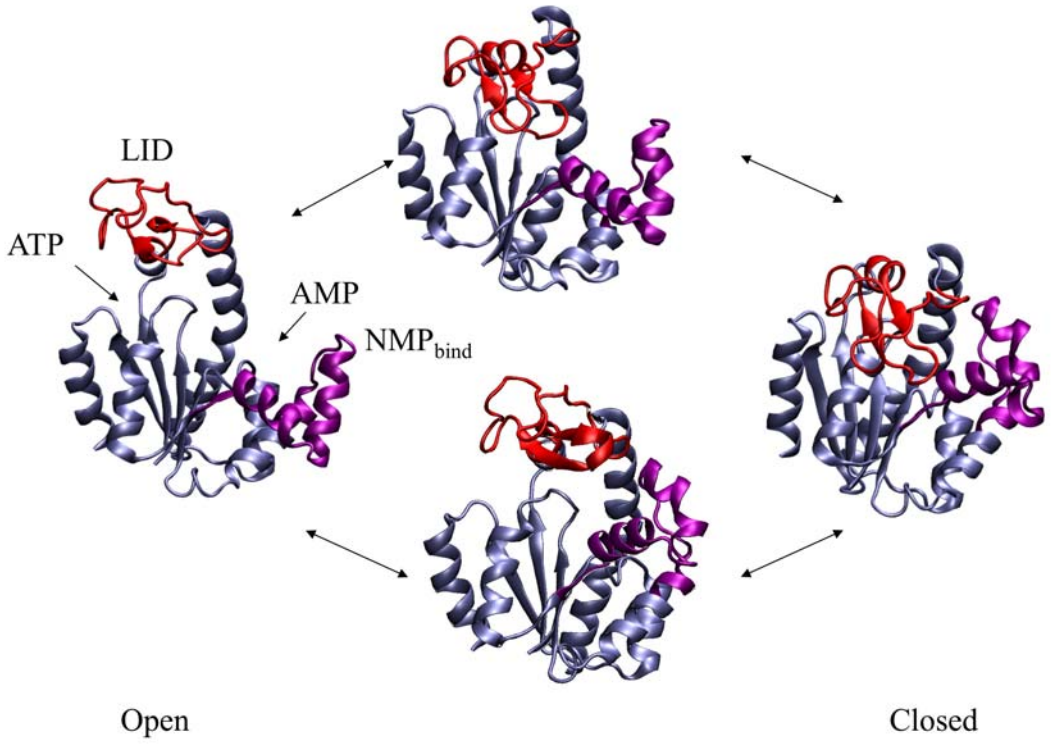

Fig. S1.—Conformational diversity of AK. *Left:* 4AKE apo crystal structure, with ATP and AMP binding pockets labeled. *Top:* A snapshot from the *t*0-open–SB simulation. The lid is closed over ATP, but the NMP_{bind} domain is open. *Bottom:* A snapshot from the *t*0-closed–apo simulation. The LID is opened, but the NMP_{bind} domain is closed. *Right:* 2ECK crystal structure with the AP5A substrate removed. The LID (*red*) and NMP_{bind} (*purple*) domains are highlighted.

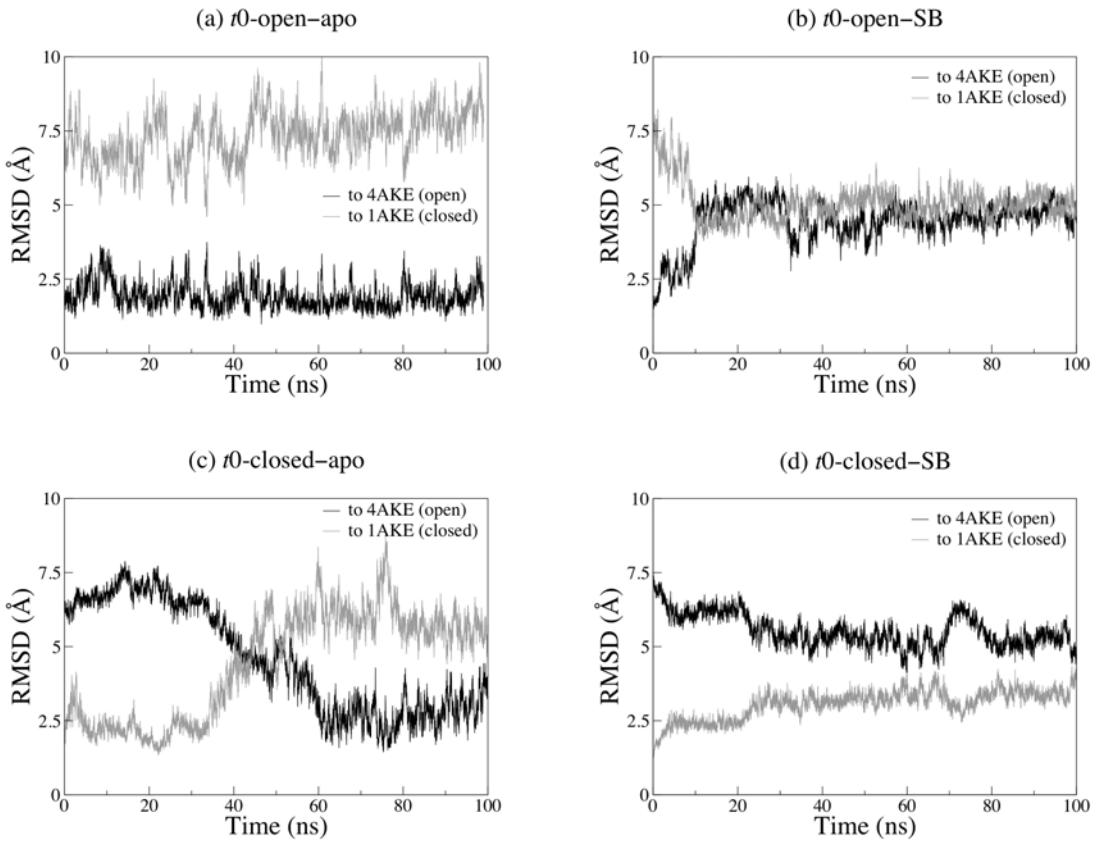

Fig. S2.—Root-mean-square distance of nonhydrogen atoms from the 4AKE (*black*) and 1AKE (*gray*) crystal structures. (*a*) *t*0-open–apo simulation. This simulation remains open for the entire 100 ns run, with a stable RMSD of ~2 Å to the open crystal structure. (*b*) *t*0-open–SB simulation. When substrates were added to the open crystal structure, the lid domain closed over ATP from 5 to 12 ns of this run, which is visible as the increase in RMSD to the open structure (*gray*) and decrease in RMSD to the closed structure (*black*). The LID domain remains closed and NMP_{bind} domain open for the rest of the simulation. (*c*) *t*0-closed–apo simulation. When substrates were removed from this crystal structure, it opened in two steps. First, the LID binding domain opened, which can be seen as a drop in RMSD to the open structure over ~20 ns from 30 to 50 ns in our simulation (*black line*). Then, over ~10 ns from 52 to 62 ns in our simulation, the NMP_{bind} domain opened. (*d*) *t*0-closed–SB simulation. AKE remained closed for the entire 100 ns simulation, although the NMP_{bind} domain fluctuated considerably giving an average RMSD to the closed structure (*gray*) of 3 Å.

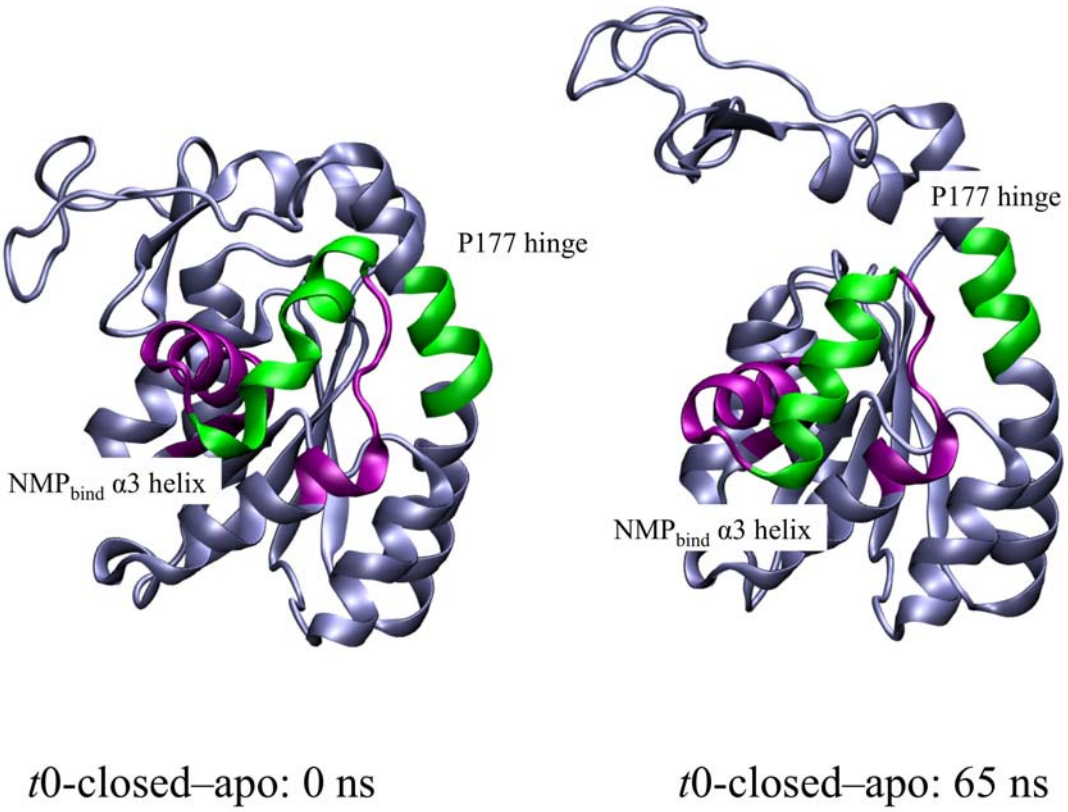

Fig. S3.—Distortion (*left*) and relaxation (*right*) of the Pro177 hinge and the α3 helix in the *t*0-closed–apo simulation.

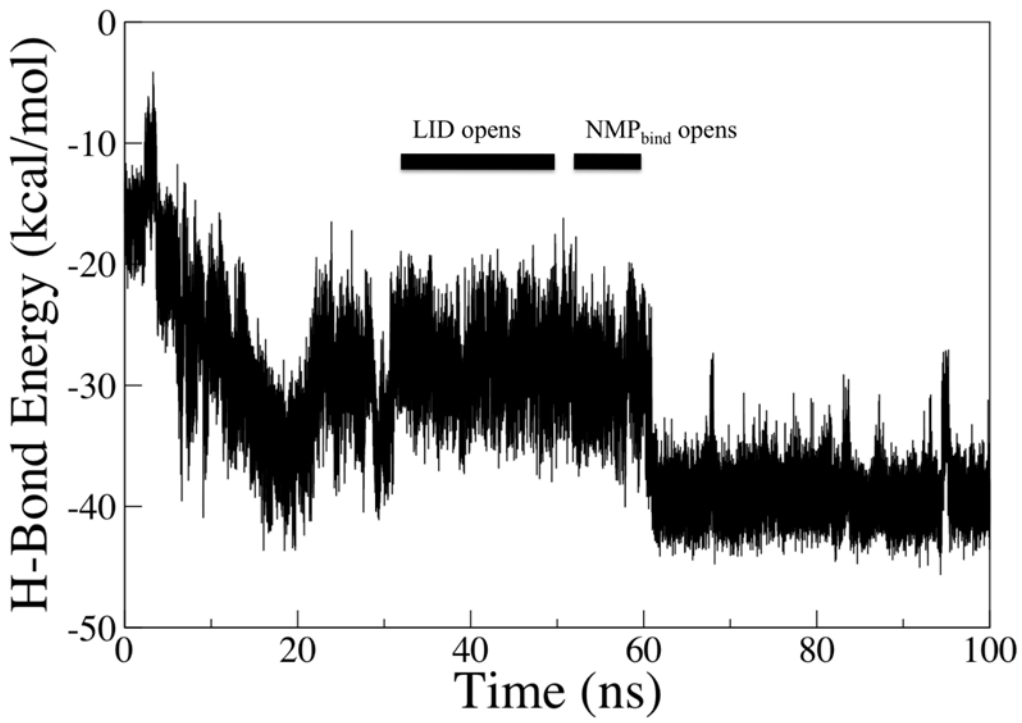

Fig. S4.—Hydrogen bond energy of between the backbone atoms in α3 helix from *t*0-closed–apo simulation. The CHARMM hydrogen-bond analysis-only parameters were used to monitor interactions among backbone atoms of AK residues 43-55. This helix went from being significantly overstretched to an intact helix, as evidenced by the decrease of ~25 kcal/mol, corresponding to 4-5 hydrogen bonds, observed in this hydrogen bonding energy over the coarse of the simulation. The helix refolding preceded NMP_{bind} domain opening, except for a final 1-2 hydrogen bonds, indicating that reducing strain on this helix is a driving force for NMP_{bind} opening.

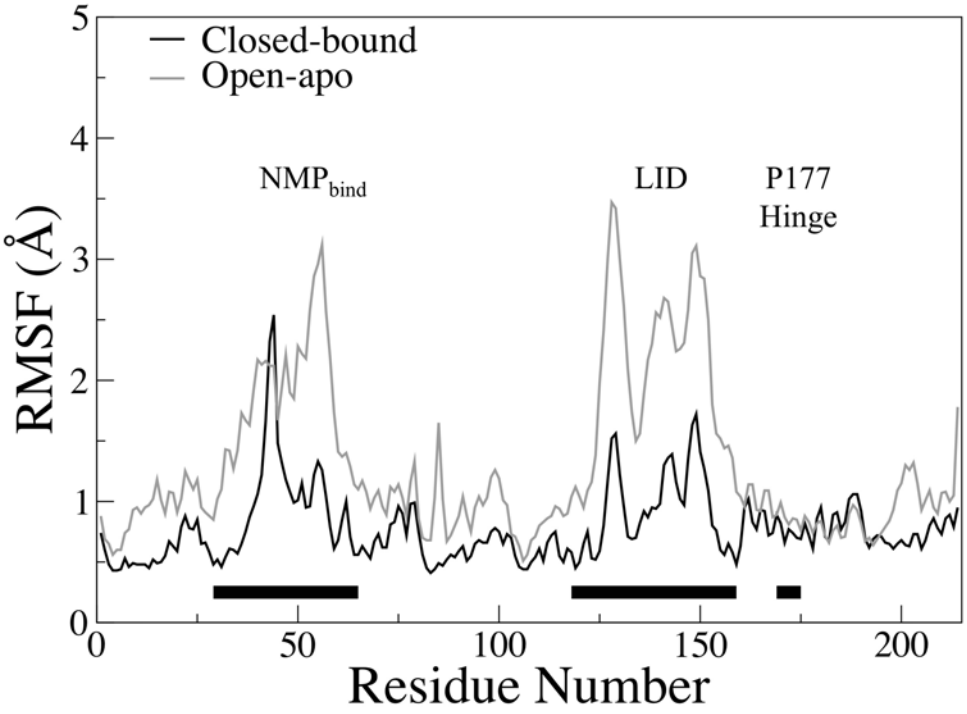

Fig. S5.—Root-mean-square fluctuations of heavy atoms by residue number. These are taken from 12 ns from the *t*0-open–apo simulation (*gray*) (AK open) and *t*0-closed–SB simulation (AK closed) (*black*). The LID (residues 118 to 159, *center bar*) and NMP_{bind} (residues 29 to 65, *left bar*) domains are readily identifiable as having higher fluctuations than the rest of the protein. A hinge region (*right bar*) is folded and shows low RMSF in both of these simulations. The *t*0-open–apo conformation has uniformly higher fluctuations, with even higher values in the domains that undergo large-scale motions in the conformational transition. These results are consistent with experimental NMR order parameter and crystal-structure *B*-factor measurements of protein fluctuations.

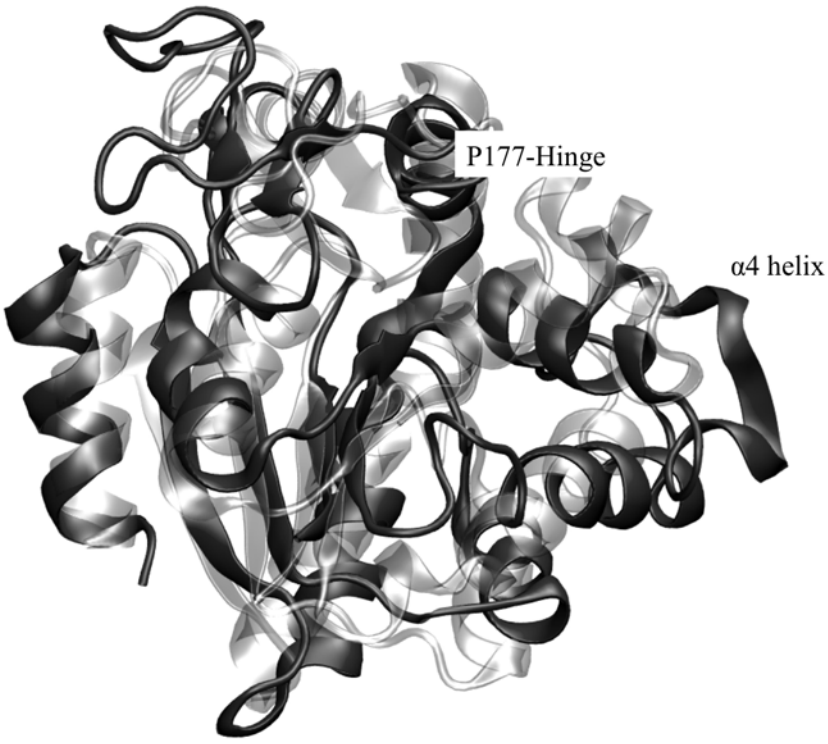

Fig. S6.—Final “closed” structure of the *t*0-closed–apo-OPLS simulation (*black*) compared to the closed 1AKE crystal structure (*transparent gray*). The *t*0-closed–apo-OPLS simulation is significantly distorted in several α helixes; the α4 and P177 hinge are highlighted. This “closed” structure has an RMSD from the 1AKE crystal structure of ~5.4 Å.

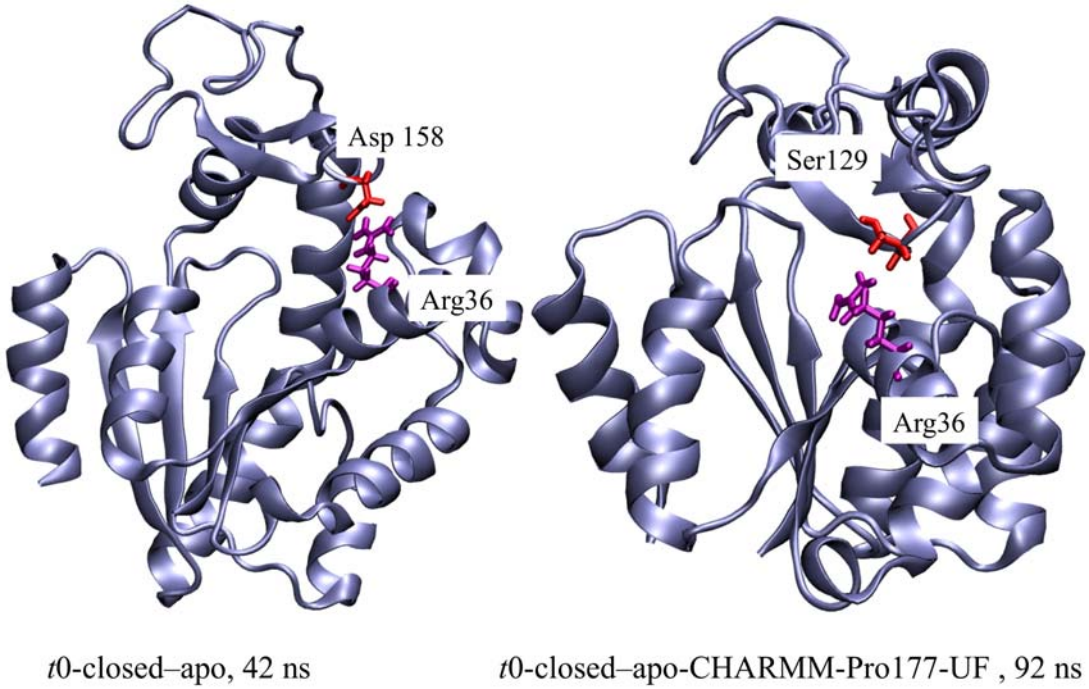

Fig. S7. —Alternate tertiary contacts formed upon the unfolding of Pro177 hinge. Arg36 in the NMP_{bind} domain contacts Asp 158 near the boundary between the LID and CORE in the *t*0-closed–apo simulation for much of the opening transition (*left*). However, in the *t*0-closed–apo-CHARMM-Pro177-UF simulation (*right*), this same residue forms a close contact with Ser 129 at the edge of the LID domain instead, which results in a different "closed" structure with a longer NMP_{bind}-CORE distance but a short NMP_{bind}-LID distance.

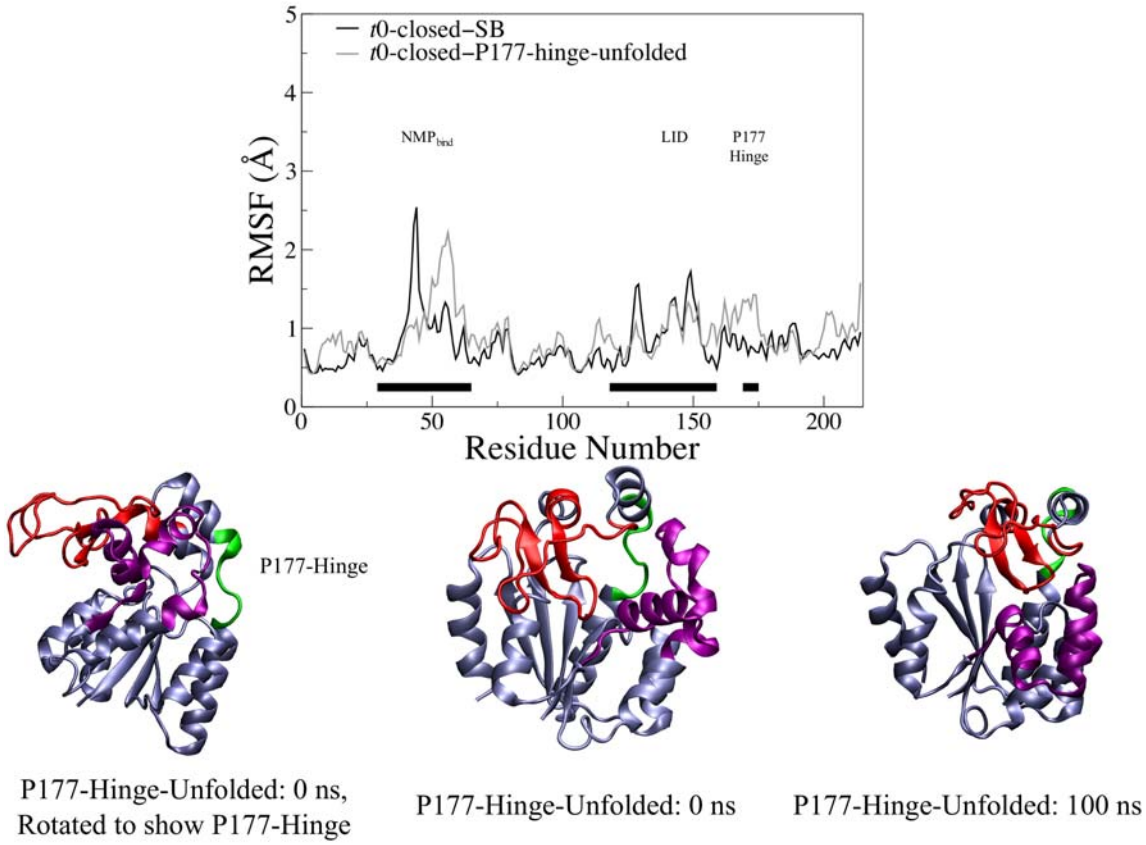

Fig. S8.—All-atom MD simulation of AK when the Pro177 hinge is in an unfolded conformation. *Top:* RMSF from 12 ns of the *t*0-closed–apo-Pro177-UF simulation (*gray*), with the *t*0-closed–SB data for comparison (*black*). The simulation shows similar fluctuations to the *t*0-closed–SB simulation, although the unfolding from r esidues 169 to 175 (*right bar*) led to a significant increase in fluctuation in this region (Fig. S5). *Bottom left:* Starting structure for the *t0*-closed–apo-Pro177-UF simulation, rotated to highlight the unfolded P177 hinge. *Bottom center:* Starting structure showing initial LID and NMP_{bind} interactions. *Bottom right:* Ending structure for the the *t0*-closed–apo-Pro177-UF simulation, showing a closed conformation with strong interactions between the LID and NMP_{bind} domains.

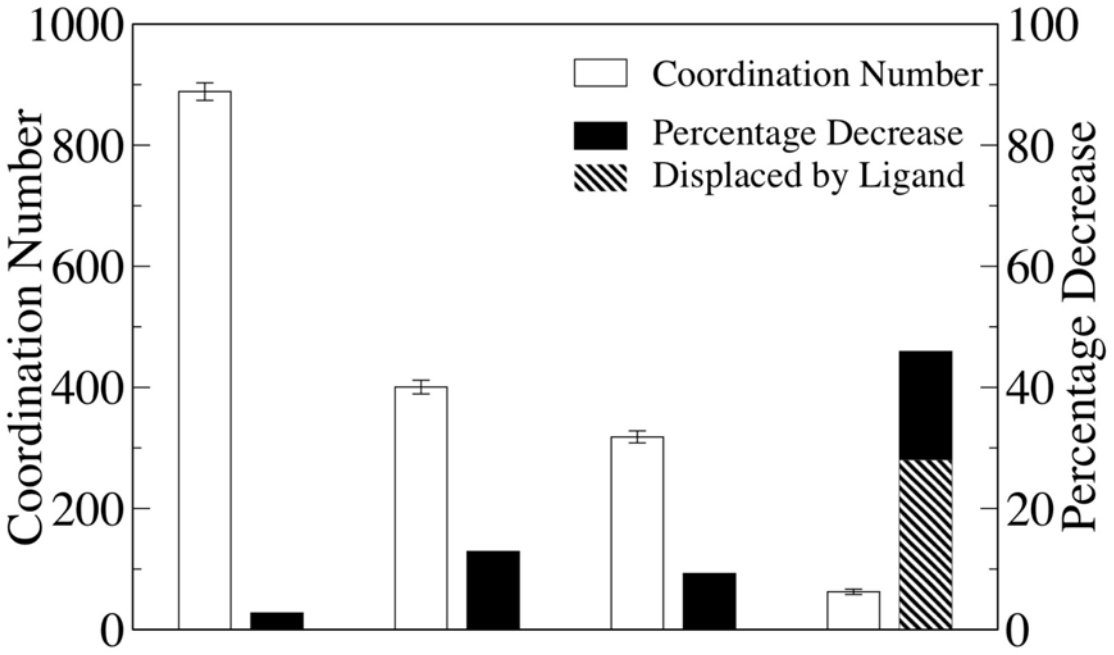

Fig. S9.—Water coordination number of the open AKE structure and its percentage change upon substrate binding and closing. Our simulations with explicit solvent allowed us to investigate detailed interactions with individual water molecules. We divided the protein into domains of different masses and sizes and counted the average number of water molecules within 5.0 Å of any protein atom for 15 ns of stable *t*0-open–apo simulation and 15 ns of stable *t*0-closed–SB simulation. The average (*open bars*) and its standard deviation (*error bars*) are plotted on the left axis, and the percentage decreases in average water coordination number (*filled bars*) are plotted on the right axis. Although the absolute numbers are not directly comparable because of the different volumes defined by each domain, the much larger percentage decrease localized on the ATP binding loop shows strong localized effects of substrate binding and conformational change in the active site. Approximately 28% of this is due to the substrate itself displacing water molecules, while the remaining 18% is due to structural differences in the closed conformation.

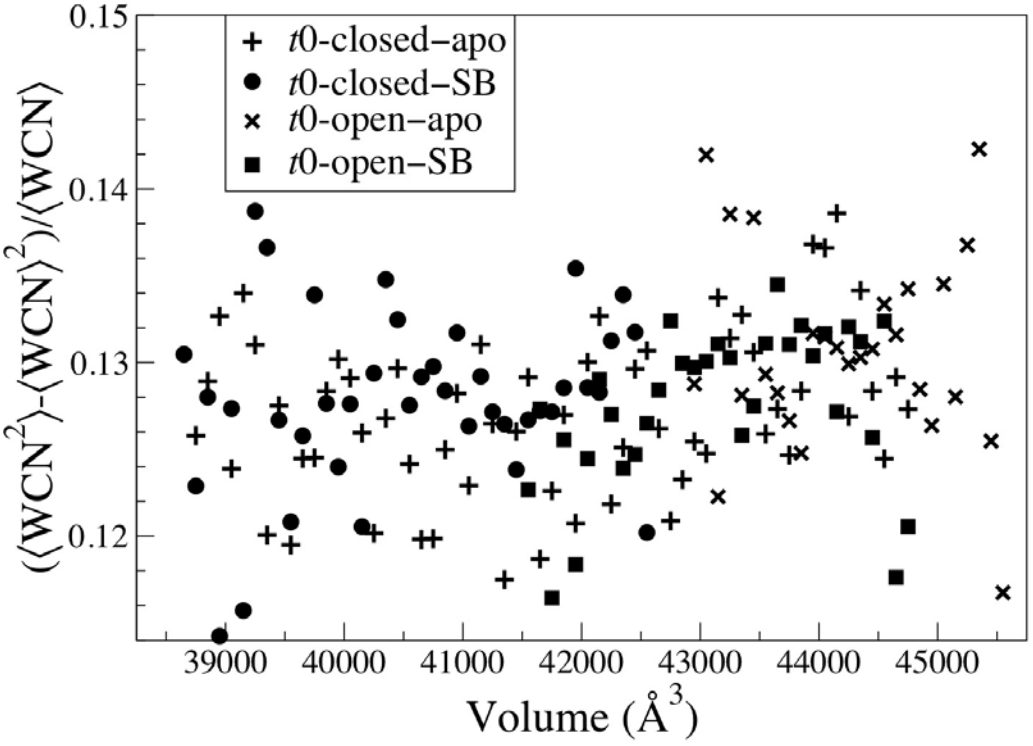

Fig. S10.—Water compressibility measured by ($\langle WCN^2\rangle$ - $\langle WCN\rangle^2$)/$\langle WCN\rangle$ in 100 Å^3 bins for each of the four simulations. Bins with <250 data points were discarded for insufficient statistics.

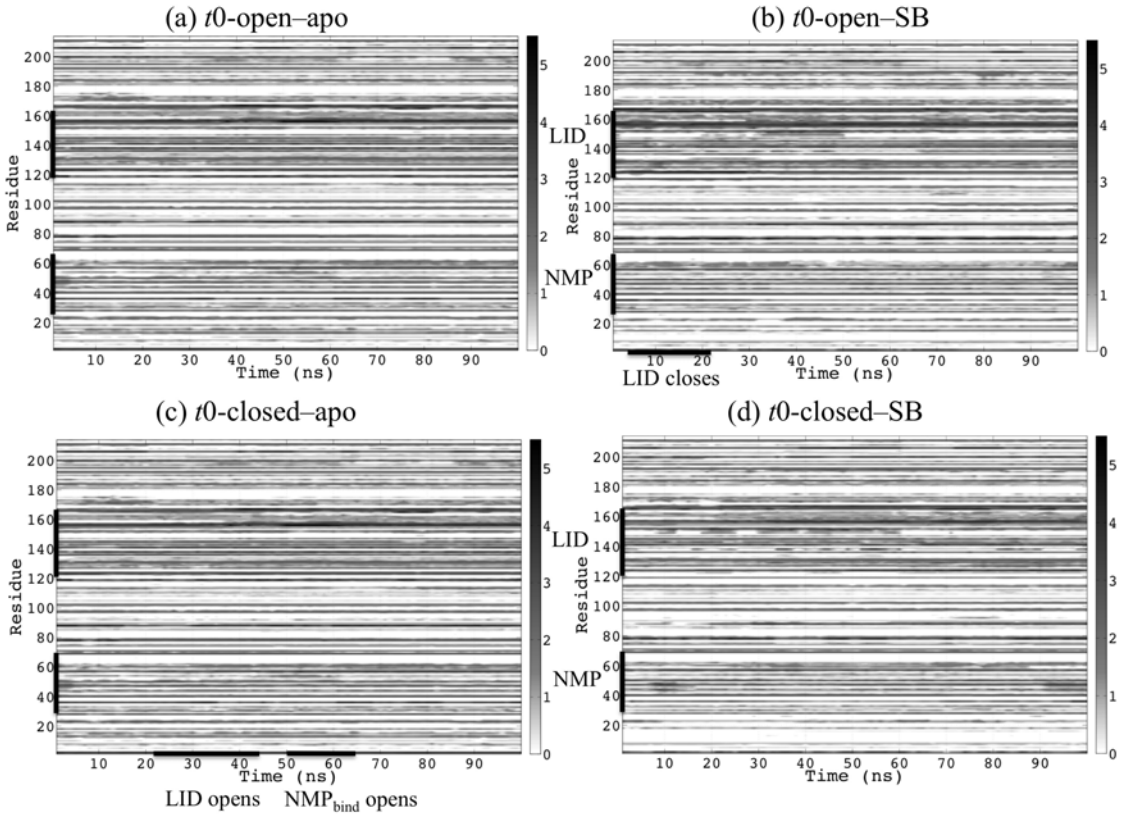

Fig. S11.—Hydrogen bond occupancy number for each residue in 1 ns bins during (*a*) *t*0-open–apo, (*b*) *t*0-open–SB, (*c*) *t*0-closed–apo, (*d*) *t*0-closed–SB simulations. LID and NMP_{bind} domains are marked, and periods of conformational change are noted in the *t*0-open–SB and *t*0-closed–apo simulations. Hydrogen bonding to the protein shows no change associated with different conformations. (*b*,*d*) The region around residue 10, the so-called ATP-binding loop, has hydrogen bonds to water that are displaced by substrate in both substrate-bound simulations. Also in the substrate-bound simulations, water forms an intermittent hydrogen bond to glutamate residue 151, which is on the top (exterior) of the LID away from the binding site. It forms a hydrogen bond to histidine residue 126 (on the interior side of the LID, but pointing out) in the open structure, but not in the closed.

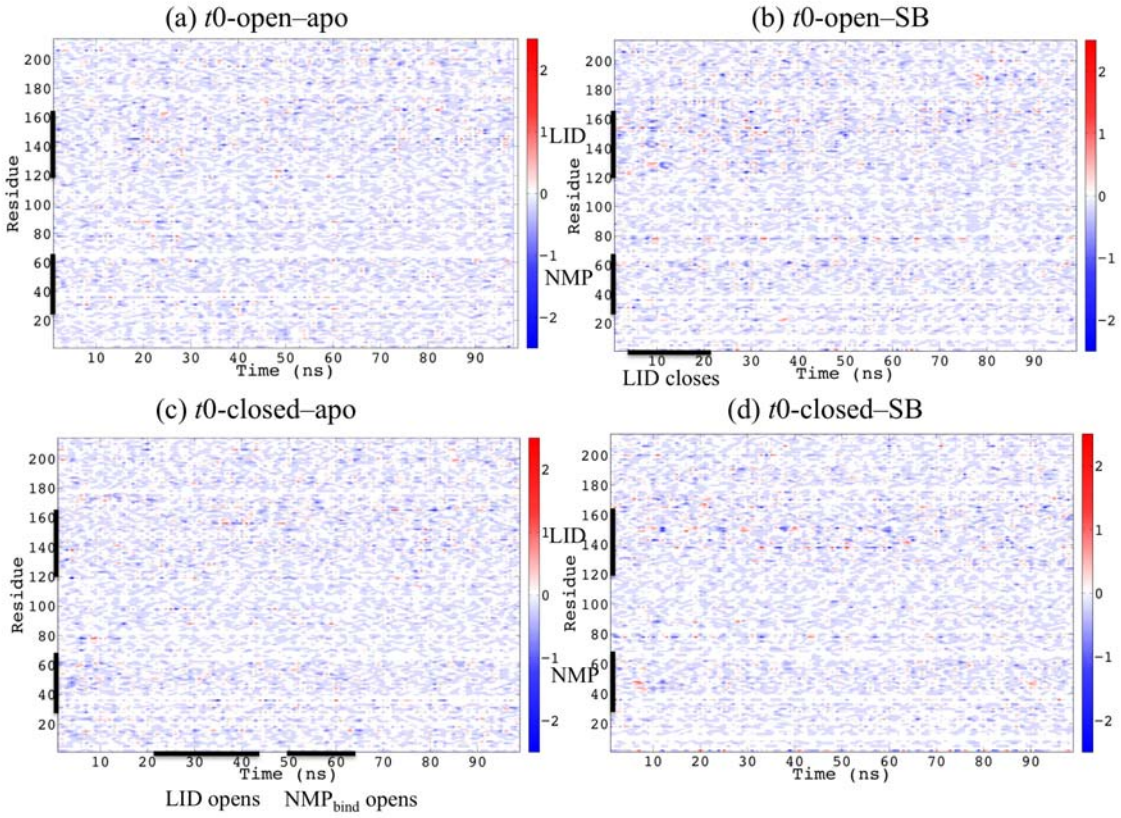

Fig. S12.—Difference in occupancy of hydrogen bonds to each residue between 1 ns segments of (*a*) *t*0-open–apo, (*b*) *t*0-open–SB, (*c*) *t*0-closed–apo, (*d*) *t*0-closed–SB simulations. LID and NMP_{bind} domains are marked, and periods of conformational change are noted in the *t*0-open–SB and *t*0-closed–apo simulations. Hydrogen bonding to the protein shows no change associated with different conformations. In addition to the intermittent changes near residue 150 discussed in Fig. S11, some intermittent hydrogen bonds to water form to arginine residue 78 on the exterior of the protein (away from the binding pockets), which otherwise forms hydrogen bonds with glutamic acid residue 75 and asparagine residue 79.

Fluctuations of AK conformation

To further quantify the structure-dependent flexibility of AK, the root-mean-square fluctuation (RMSF) of each heavy atom is calculated from portions of simulations that stay in the closed or open conformation; in particular, from the structures sampled in 12 ns subtrajectories of the *t*0-closed–SB and *t*0-open–apo simulations. The results are shown in Fig. S5, and the profiles of RMSF are consistent with those of experimental NMR order parameters (1, 2) and crystal structure *B*-factors (3, 4). The LID and NMP_{bind} domains are more flexible than other parts of the protein in both open and closed forms. In the open form, the LID domain is more flexible than the NMP_{bind} domain and becomes similarly or slightly less flexible than NMP_{bind} upon closing (Fig. S5). The higher flexibility of the LID in open AK corresponds to a higher susceptibility to protein-substrate interactions, and the LID-closes-first mechanism is thus observed in the *t*0-open–SB simulation. The relaxing of overstretched α3 from closed to open also caused significant changes in the distribution of RMSF within the NMP_{bind} domain.

All-atom MD simulation of AK using the OPLS force field and the local unfolding of Pro177 hinge

The various stabilities of α helixes encoded in all-atom force fields (5) may lead to different structures of the Pro177 hinge and could be exploited as a tool to sample different mechanisms of the closed-to-open transition. Therefore, we further examine the coupling between the Pro177 hinge and the closed-to-open transition of AK by using a different force field to perform the *t*0-closed–apo simulation. In particular, we apply the OPLS force field (6) and compare the resulting *t*0-closed–apo-OPLS simulation with the *t*0-closed–apo-CHARMM simulation presented in the text. In the *t*0-closed–apo-CHARMM simulation, the LID domain opened first followed by the NMP_{bind} domain (Fig. 2), and the distorted helix near Pro177 quickly straightened into a more intact helix (Fig. S3). In the *t*0-closed–apo-OPLS simulation, on the other hand, the distorted helix near Pro177 (residues 169-175) unfolded. As a result, the LID-to-CORE distance underwent large fluctuations, sampling values that correspond to those of closed and open X-ray structures. After the Pro177 hinge unfolded in the *t*0-closed–apo-OPLS simulation, the organization between LID, NMP_{bind}, and CORE domains is also altered because of a more extended Pro177 hinge. At the end of the *t*0-closed–apo-OPLS simulation, AK arrived at a structure with short LID-to-CORE distance but with a RMSD = 5.4 Å to 1AKE (Fig. S6). LID opening only transiently occurred in the *t*0-closed–apo-OPLS simulation, and alternative structural changes in AK conformation occurred in responding to the absence of protein-substrate interactions in the closed form.

The result that the Pro177 hinge spontaneously unfolded in the *t*0-closed–apo-OPLS simulation but not in the *t*0-closed–apo simulation using the CHARMM force field indicates the distinct stabilities of secondary structures encoded in different atomic force fields (5, 7). Furthermore, interresidue interactions and hence AK structures after the Pro177 hinge is unfolded are also force-field dependent. Despite these discrepancies, the result that the local unfolding of Pro177 hinge hinders the closed-to-open transition of AK is robust.

The solvation structures surrounding AK during open-to-closed and closed-to-open transitions

To characterize the water coordination numbers (WCNs) of AK in the open and closed forms, WCNs calculated from the transitionless segments (15 ns) in the *t*0-open–apo (AK open) and *t*0-closed–SB (LID and NMP_{bind} both closed) simulations are compared. The total WCN (water molecules with oxygen within 5.0 Å of any protein atom) of open AK is 1492 ± 20 and is only ~10% higher than that (1338 ± 19) of the closed AK. Decomposing WCNs into contributions from LID, NMP_{bind}, and CORE domains show a 5-10% reduction. Around the ATP binding loop (residues 8-15), on the other hand, an average WCN of 62 ± 4 is found in the open but only 34 ± 3 in the closed form, a 46% difference (Fig. S9). However, about 17 (~28%) of this reduction in WCN is due to the exclusion of water molecules by substrates. Therefore, the reduction in WCN around the ATP binding region due to conformational change is ~11 (18%). Thus, the change in solvation due to conformational change is rather homogeneous across different domains (~10 % reduction in WCN upon closing), with a more significant change in the catalytic pocket of AK (18% reduction in WCN upon closing).

The above comparison in WCN is between AK conformations that are fully open and closed (both LID and NMP_{bind} domains). A similar pattern of changes in WCN is also observed as a result of the structural transition observed in the *t*0-closed–apo simulation (Fig. 4). The WCN increased from a 5-ns-block-average (symmetric around a given time) of 1337 at 12.5 ns (before opening) to 1474 at 97.5 ns. The partial opening of the NMP_{bind} domain observed in the *t*0-closed–SB simulation is also associated with an increase in WCN from 1334 at 12.5 ns to 1416 at 97.5 ns. In the *t*0-open–SB simulation, on the other hand, LID closing (NMP_{bind} remained open) did not lead to a noticeable decrease in overall WCN; the 5-ns-block-average of WCN at 2.5 ns is 1483 versus 1438 at 97.5 ns. However, the 5-ns-block-averaged WCN of ATP did show a decrease from 53 at the 7.5 ns to 40 at the 17.5 ns as the LID closed over ATP in the *t*0-open–SB simulation. This 24% decrease in the ATP WCN reiterates our finding of a larger local WCN decrease in the binding pocket when comparing *t*0-open–apo and *t*0-closed–LB simulations (Fig. S9).

METHODS

To perform all-atom MD simulations of AK, the starting configurations are taken from the crystal structures of AK in the protein data bank as discussed. Coordinates that are missed in X-ray structures were generated using the internal coordinate facilities of CHARMM (8). Potassium chloride was used to neutralize the system (23 K^+ and 18 Cl^- for simulations without and 22 K^+ and 13 Cl^- for simulations with substrates). The positions of ions were obtained using the Solvate 1.0 program (9). The proteins and ions were then placed in a pre-equilibrated water box with the TIP3P explicit water model (10); water molecules within ~2.4 Å of protein atoms or ions were removed. The final systems without substrates contained 32,129 atoms, with 3345 atoms for AK, 41 ions, and 28,743 water atoms. The systems with substrates contain 32,193 atoms, with 3345 atoms for AK, 35 for AMP, 43 for ATP, 1 Mg^{2+}, 35 K^+ and Cl^-, and 28,734 water atoms.

The NAMD software (11) was used to perform the molecular dynamics simulations of all simulations with periodic boundary conditions. The CHARMM22 (7) all-atom force field with the CMAP cross terms (5, 7) was used to compute the potential energy. The OPLS force field (6) was used for one of the simulations, as discussed in the text. Long-range electrostatic interactions were computed using the particle mesh Ewald algorithm (12). Covalent bonds to hydrogen were constrained to their equilibrium values by the SHAKE algorithm (13), allowing an integration time step of 2 fs. The structures were minimized with at least 60,000 conjugate gradient steps, with protein backbone atoms restrained to their original positions using harmonic potentials with a force constant of 1.0 kcal/mol/Å. The system was then heated to 300 K by reassigning velocities every 0.2 ps at a rate of 30 K/ps. After reaching 300 K, the systems were allowed to equilibrate at 300 K and 1 atm for 1 ns in the presence of restraint potentials. The temperature was controlled with a Langevin thermostat with a 0.5 ps^{-1} damping coefficient, and the pressure was controlled by a Langevin-piston barostat (14) with a piston period of 2 ps and a damping time constant of 2 ps. The restraint potentials were then removed in production runs after the equilibration period. In order to characterize the structural properties of AK, coordinates of the system were saved every 500 steps (1 ps) for analysis. Visualization of protein structures was performed with the Visual Molecular Dynamics (VMD) program (http://www.ks.uiuc.edu/Research/vmd/ (15)).

The backbone unfolding near proline residue 177 was achieved by taking as a target structure the backbone coordinates of an unfolded coil configuration from an unrelated simulation. These coordinates were used in place of the crystal structure coordinates for residues 169 through 175. The structure was then solvated as usual, then minimized for 100,000 conjugate gradient steps with the usual harmonic constraints to the crystal structure positions removed for residues 161 through 188. This structure was heated and then extensively equilibrated with the same constraints for 11 ns of simulation time, which was necessary to avoid nonequilibrium behavior with this modified starting structure.

For the mutant yeast and bovine AK crystal structures (16, 17), the respective NMP_{bind}-CORE and LID-CORE distances presented in Fig. 2 were determined by

aligning structures to identify the appropriate interresidue distances. For the mutant yeast AK, PDB ID 1DVR, the LID-CORE distance was that between C_α's of residues Ala198 and Pro136, and the NMP_{bind}-CORE distance was between Gln59 and Ala178. For the bovine AK, PDB ID 2AK3, the LID-CORE distance was between Glu192 and Pro130, and the NMP_{bind}-CORE was between Gln60 and Lys172.

Hydrogen bond analysis with CHARMM (Fig. S4) (8) was performed with an analysis-only force field with explicit hydrogen bonding terms. Coordinates sampled from MD simulations were used for analysis.

REFERENCES

1. Shapiro, Y. E., E. Kahana, V. Tugarinov, Z. C. Liang, J. H. Freed, and E. Meirovitch. 2002. Domain flexibility in ligand-free and inhibitor-bound Escherichia coli adenylate kinase based on a mode-coupling analysis of N-15 spin relaxation. Biochemistry 41:6271-6281.
2. Shapiro, Y. E., M. A. Sinev, E. V. Sineva, V. Tugarinov, and E. Meirovitch. 2000. Backbone dynamics of Escherichia coli adenylate kinase at the extreme stages of the catalytic cycle studied by N-15 NMR relaxation. Biochemistry 39:6634-6644.
3. Muller, C. W., G. J. Schlauderer, J. Reinstein, and G. E. Schulz. 1996. Adenylate kinase motions during catalysis: An energetic counterweight balancing substrate binding. Structure 4:147-156.
4. Muller, C. W., and G. E. Schulz. 1992. Structure of the Complex between Adenylate Kinase from Escherichia-Coli and the Inhibitor Ap5a Refined at 1.9 a Resolution - a Model for a Catalytic Transition-State. J. Mol. Biol. 224:159-177.
5. Mackerell, A. D., M. Feig, and C. L. Brooks. 2004. Extending the treatment of backbone energetics in protein force fields: Limitations of gas-phase quantum mechanics in reproducing protein conformational distributions in molecular dynamics simulations. J. Comput. Chem. 25:1400-1415.
6. Jorgensen, W. L., D. S. Maxwell, and J. TiradoRives. 1996. Development and testing of the OPLS all-atom force field on conformational energetics and properties of organic liquids. J. Am. Chem. Soc. 118:11225-11236.
7. MacKerell, A. D., D. Bashford, M. Bellott, R. L. Dunbrack, J. D. Evanseck, M. J. Field, S. Fischer, J. Gao, H. Guo, S. Ha, D. Joseph-McCarthy, L. Kuchnir, K. Kuczera, F. T. K. Lau, C. Mattos, S. Michnick, T. Ngo, D. T. Nguyen, B. Prodhom, W. E. Reiher, B. Roux, M. Schlenkrich, J. C. Smith, R. Stote, J. Straub, M. Watanabe, J. Wiorkiewicz-Kuczera, D. Yin, and M. Karplus. 1998. All-atom empirical potential for molecular modeling and dynamics studies of proteins. J. Phys. Chem. B 102:3586-3616.

8. Brooks, B. R., R. E. Bruccoleri, B. D. Olafson, D. J. States, S. Swaminathan, and M. Karplus. 1983. Charmm - a Program for Macromolecular Energy, Minimization, and Dynamics Calculations. J. Comput. Chem. 4:187-217.
9. Grubmüller, H. 1996. Solvate 1.0. In Solvate 1.0. Max Planck Institute for Biophysical Chemistry, Göttingen.
10. Jorgensen, W. L., J. Chandrasekhar, J. D. Madura, R. W. Impey, and M. L. Klein. 1983. Comparison of Simple Potential Functions for Simulating Liquid Water. J. Chem. Phys. 79:926-935.
11. Nelson, M. T., W. Humphrey, A. Gursoy, A. Dalke, L. V. Kale, R. D. Skeel, and K. Schulten. 1996. NAMD: A parallel, object oriented molecular dynamics program. Int. J. Supercomput. Appl. High Perform. Comput. 10:251-268.
12. Darden, T., D. York, and L. Pedersen. 1993. Particle Mesh Ewald - an N.Log(N) Method for Ewald Sums in Large Systems. J. Chem. Phys. 98:10089-10092.
13. Allen, M. P., and D. J. Tildesley. 1987. Computer Simulations of Liquids. Oxford Univ. Press, New York.
14. Feller, S. E., Y. H. Zhang, R. W. Pastor, and B. R. Brooks. 1995. Constant-Pressure Molecular-Dynamics Simulation - the Langevin Piston Method. J. Chem. Phys. 103:4613-4621.
15. Humphrey, W., A. Dalke, and K. Schulten. 1996. VMD: Visual molecular dynamics. J. Mol. Graphics 14:33-&.
16. Diederichs, K., and G. E. Schulz. 1991. The Refined Structure of the Complex between Adenylate Kinase from Beef-Heart Mitochondrial Matrix and Its Substrate AMP at 1.85 A Resolution. J. Mol. Biol. 217:541-549.
17. Schlauderer, G. J., K. Proba, and G. E. Schulz. 1996. Structure of a mutant adenylate kinase ligated with an ATP-analogue showing domain closure over ATP. J. Mol. Biol. 256:223-227.